Nanoscale

PAPER

View Article Online
View Journal | View Issue

Cite this: *Nanoscale*, 2019, **11**, 20977

Rapid template-free synthesis of nanostructured conducting polymer films by tuning their morphology using hyperbranched polymer additives†

Chun-Fu Lu, [a] Song-Fu Liao,[a,b] Ke-Hsin Wang,[a] Chin-Ti Chen, [b] Chi-Yang Chao[a] and Wei-Fang Su *[a]

Received 19th June 2019,
Accepted 7th October 2019

DOI: 10.1039/c9nr05218f

rsc.li/nanoscale

Nanostructures in conducting polymer films can enhance charge carrier and ion transfer, provide porosity with high specific area and confer unique optoelectronic properties for potential applications. A general and facile synthesis has been developed to prepare nanostructured conducting polymer films without the need for using templates. This simple approach employs hyperbranched polymers as additives to tune the morphology of conducting polymer films into a continuous nanofibril network. Nanostructured conducting polymer films with improved crystallinity exhibit good charge carrier transport and stable nanofibril network, without sacrificing either property upon removing residual additives. Polymer field-effect transistor sensors have been used to demonstrate the benefits of the large surface area provided by the nanofibril network. The sensors with porous nanostructures exhibit lower detection limits (two times lower) and faster response times (33% faster) compared to the sensors without nanostructures. This general approach can advance the knowledge and development of nanostructured conducting polymer films for energy harvesting and storage, electronics, catalysts, sensors and biomedical applications.

Introduction

Conducting polymers (CPs) have evolved from mere theoretical concepts to rising organic semiconductors with mobility rivaling amorphous silicon in the past few decades. Much interest in synthesizing CPs with nano-scaled structures is driven by tuning the intrinsic properties of CPs and exploring the potential of CPs in new avenues. Nanostructured CPs have attractive functionalities such as high carrier mobility, large surface area, efficient diffusion pathway, electrochemical activity and mechanical properties, enabling their numerous applications in energy harvesting, energy storage, soft electronics, sensors and biomedical fields.[1–9] Hence, various approaches[10,11] have been developed to introduce nanostructures into CPs, mainly *via* a bottom-up fashion. The controlled synthesis of nanostructured CPs can be categorized into two approaches: the template-based synthesis and the template-free synthesis. The widely adopted template-based synthesis employs templates such as polyester membranes, anodic aluminum oxide membranes, zeolites, metal oxides, lyotropic liquid crystals, DNA and ionic liquids,[10] to tune the morphology of CPs and form nanostructures. Various nanostructured conducting polymers have been reported in the literature such as poly(3,4-ethylenedioxythiophene) nanowires, polyaniline nanotubes, polypyrrole nanospheres and polyindole nanowires.[12–16] However, the approach suffers from the drawbacks of tedious multi-step synthesis routes and the deformation of nanostructures upon removing the pre-modified template. A simple and straightforward solution lies in template-free synthesis, including interfacial polymerization, conducting polymer hydrogels, electrospinning and conducting polymer nanocomposites.[7,17–19] Among the listed methods, only conducting polymer nanocomposites can produce stable and versatile nanostructures with conducting polymers with high degree of polymerization and low molecular weight distribution. Nanocomposites of pre-synthesized conducting polymers and insulating polymers can form nanostructures *via* nanoscale phase separation. Nanofibers have been incorporated into the films of poly(3-hexylthiophene), poly[(5,5′-bis(3-dodecyl-2-thienyl)-2,2′-bithiophene)], poly(diketopyrrolopyrrole-*co*-thienovinylthiophene) and other donor–acceptor conducting polymers by blending with insulating polymers such as polystyrene, poly(methyl methacrylate),

[a]*Department of Materials Science and Engineering, National Taiwan University, Taipei 10617, Taiwan. E-mail: suwf@ntu.edu.tw*
[b]*Institute of Chemistry, Academia Sinica, No. 128, Academia Road, Sec. 3, Taipei 11529, Taiwan*

†Electronic supplementary information (ESI) available. See DOI: 10.1039/c9nr05218f

poly(dimethylsiloxane), polyester and other additives.[20–25] Solvent additives like 1,8-diiodooctane, 1,8-octanedithiol, diphenyl ether, anisole and 1-chloronaphthalene are commonly used to tune the film morphology *via* fine controlling the phase separation process.[26–30] However, most of the studies only obtain nanostructured conducting polymers in compact films instead of porous films. There are more elegant ways to obtain nanostructured conducting polymers, by block copolymerizing them with coil polymers such as poly-2-vinylpyridine, poly(methyl methacrylate), *etc*.[31–33] They can self-assemble into various nanostructures by phase separation. However, most of them either do not remove the insulating components or encounter the deformation of nanostructures, decreasing the electrical properties.

Herein, we propose an alternative template-free synthesis for porous nanostructured conducting polymer films. This facile approach involves two steps: (1) spin-coating a conducting polymer solution containing spherical polymer additives to form nanostructured fibrous thin films and (2) using solvent wash or heat to remove the residual additives completely to form porous nanostructured conducting polymer films. The presence of spherical polymer additives in the conducting polymer solution is critical in this synthesis. The hyperbranched polymers are known to have low viscosity due to their non-tangling characteristics of spherical structure.[34–36] They have been widely used as viscosity control additives for conventional polymer processing.[37] We applied this known knowledge to make porous nanostructured conducting polymer films. The spherical or ellipsoidal-shaped additives exhibit no chain entanglement characteristic and can be easily removed by shear force, solvent or heat because they are not entangled with the conducting polymer. Then a film with a continuous nanofibril conducting network is formed. This approach is successfully applied to various conducting polymer blends containing hyperbranched polyesteramide (HBPEA). Isoindigo-based conducting polymers are selected for this study due to their easy synthesis and high charge carrier mobility.[38–40] Three isoindigo-based conducting polymers P4TIH, P4TIN and P4TIF are investigated. The chemical structure of conducting polymers and additives is shown in Fig. 1(a). Although hyperbranched polymers do not have an ideal spherical structure like dendrimers, they are generally cheaper and easier to synthesize compared to dendrimers. Coconut fatty acid ester (about 80%) end groups in the investigated HBPEA provide good compatibility with a variety of organic solvents and conducting polymers, enabling the formation of nanoscale morphology in the blend of conducting polymers and HBPEA. HBPEA can be partially removed by shear force during the spin-coating process and then completely removed by either acetone washing or thermal annealing (TA). A continuous nanofibril network of a polymer film was formed without any damage to the nanostructure after remov-

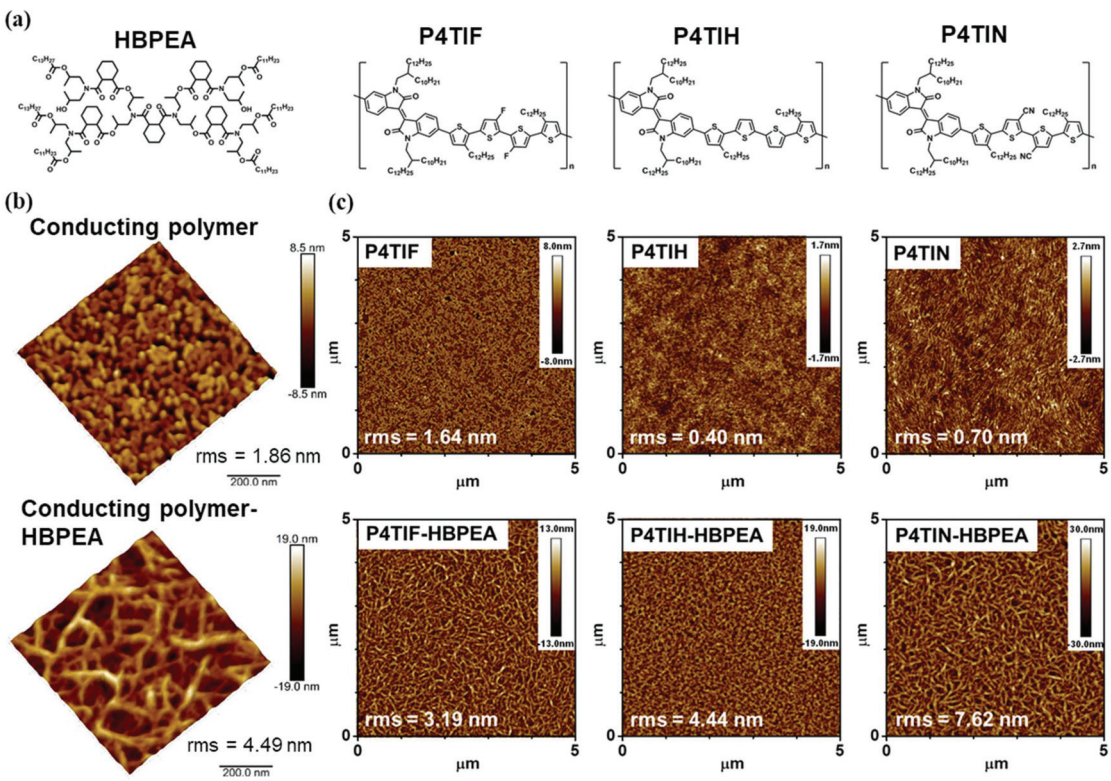

Fig. 1 Formation of nanostructured conducting polymer thin films. (a) Chemical structures of HBPEA, P4TIF, P4TIH and P4TIN. (b) 3D AFM topography images of the polymer film and conducting polymer-HBPEA film. (c) AFM height images of neat polymer films (P4TIF, P4TIH and P4TIN) and CP-HBPEA films (P4TIF-HBPEA, P4TIH-HBPEA and P4TIN-HBPEA).

ing additives. The electrical properties of the films were characterized by the field-effect transistor (FET) structure. The FETs fabricated from continuous nanofibril network films show mobility and field-effect similar to the device fabricated with densely packed polymer films. The porous nature of the nanostructured thin films is particularly beneficial for the applications requiring high surface area such as sensors and catalysts. We demonstrate that a P4TIF polymeric FET sensor with a continuous nanofibril network exhibits faster and larger response by employing this method. The device can detect 100 ppb ammonia in air in less than 26 s. These results provide guidelines for synthesizing conducting polymer thin films with stable continuous nanofibril networks without sacrificing intrinsic electrical properties.

Results and discussion

The high mobility isoindigo-based conducting P4TIX polymers (P4TIH, P4TIN and P4TIF) were synthesized *via* Stille coupling of bithiophene-flanked isoindigo and the corresponding functionalized bithiophene, according to our previous report.[41–43] The hyperbranched polyesteramide (HBPEA) used in this study features a moderate molecular weight of 2600 Da, suitable for the formation of a bi-continuous morphology in polymer blends.[44] Conducting polymers were blended with HBPEA in an equal weight ratio in chloroform and the films prepared by spin-casting are denoted as CP-HBPEA. The hyperbranched polymer has an ellipsoidal shape due to its radiant and dendrimer-like chemical structure. The non-linear molecular shape and relatively small molecular weight of HBPEA prevent chain entanglement commonly occurring in polymer–polymer blends. Both polymers and additives contain long alkyl chains, as shown in Fig. 1(a), without heavy chain entanglement. We speculate that HBPEA does not intertwine with conducting polymers but HBPEA molecules are slightly stuck to the alkyl side chains of conducting polymers. A more detailed explanation is provided in the discussion of atomic force microscope (AFM) data and grazing-incidence wide-angle X-ray scattering (GIWAXS) data below. When conducting polymers aggregate during the film deposition process, phase separation occurs concurrently in nanometer scale under the applied shear force and solvent evaporation. Thus, nanostructures are initiated and formed in conducting polymer films by removing HBPEA which surrounds the conducting polymer aggregates.

An atomic force microscope was used to investigate the nanoscale phase separation by probing the surface morphology of the conducting polymer films. The 3D topography images of the neat conducting polymer film and the CP-HBPEA film are shown in Fig. 1(b), and P4TIX represents the conducting polymer in these images. The neat conducting polymer film contains a smooth surface dotted with spherical aggregates of the polymer. This kind of surface morphology is usually observed in neat conducting polymer films.[38,45,46] In contrast, the CP-HBPEA film exhibits intricate structures of nanofibers with diameter ranging from 15 to 40 nm. From the visualized 3D image, the nanofibers are interconnected three-dimensionally to form a continuous nanofibril network instead of an array of nanofibers in a single plane. Such nanostructures provide high porosity and large surface area, leading to a surface roughness of 4.5 nm in the CP-HBPEA film, which is two times larger than that of the neat conducting polymer film, 1.7 nm.

Blending the conducting polymer with the hyperbranched polymer is a general method to introduce a fibril network into conducting polymer thin films. Besides the demonstrated P4TIF, the other two conducting polymers P4TIH and P4TIN are blended with HBPEA in an equal weight ratio of polymers/additives, and the prepared thin films are denoted as PnTIX-HBPEA. To show that the observed nanostructure is not supported by the additives, the as-cast PnTIX-HBPEA films were dipped in acetone for 15 min to remove the residual HBPEA from the films. AFM height images of neat PnTIX films and PnTIX-HBPEA films are shown in Fig. 1(c). The AFM height image of the neat P4TIF film complements the 3D topography image: the surface of the neat P4TIF film consists of spherical P4TIF aggregates without any specific long-range order. On the other hand, the P4TIF-HBPEA film exhibits the topography of a continuous nanofibril network. The nanostructures dominate the surface morphology of the P4TIF-HBPEA film. The image was taken after the film was washed with acetone, indicating that the continuous nanofibril network in the P4TIF-HBPEA film is very stable and does not deform upon subjecting to chemicals like acetone. Similar to the neat P4TIF film, the surface of the neat P4TIH film consists of spherical aggregates, but P4TIH aggregates are generally positioned closer to each other compared to P4TIF aggregates. In the P4TIH-HBPEA film, the continuous network is constructed from P4TIH fibers uniformly present throughout the film. Compared to P4TIF-HBPEA, the length of P4TIH nanofibers is shorter (average length of 100 nm) and the voids between fibers are of smaller size (50 nm in diameter). In the case of P4TIN, polymer nanorods with a diameter of 40 nm are present in the neat P4TIN film, but the structure lacks continuity and extension in three dimensions. The rod-like structures of P4TIN aggregates are like surface features, which account for the low surface roughness of 0.70 nm. The shape of polymer aggregates, however, proved to be an insignificant factor for introducing nanostructures into conducting polymer films by blending with the hyperbranched polymer. After blending with HBPEA, P4TIN film with a continuous fibril network can be obtained, as exhibited in P4TIN-HBPEA film. The conducting polymer nanofibers are predominantly interconnected in a 3D network when prepared *via* the nanoscale phase separation of the conducting polymer and HBPEA additive. Similar nanostructures in a simple and efficient manner could be not achieved by conventional methods.

Self-supported nanostructured conducting polymer films are generally considered suitable for exploring their intrinsic properties directly in applications. Herein, we propose two simple methods to remove the hyperbranched polymer additives from the films while keeping the nanostructure of the

polymer intact: (1) washing the film using an orthogonal solvent of the conducting polymer or (2) applying thermal treatment near the decomposition temperature (T_d) of the hyperbranched polymer. P4TIF-HBPEA was used to demonstrate the aforementioned methods by investigating the as-cast film (P4TIF-HBPEA_ac), the acetone washed film (P4TIF-HBPEA_w) and the thermally annealed film (P4TIF-HBPEA_TA). HBPEA shows good solubility in various organic solvents such as chloroform, acetone and methyl ethyl ketone, because of its attached alkyl chains and moderate molecular weight. This opens up the opportunity of using chemical solvents in which P4TIF is insoluble to remove the additives. Another key factor is that the nanofibril network is not constructed or supported by HBPEA. We have proposed that HBPEA simply surrounds the conducting polymer aggregates during phase separation due to the ellipsoidal shape, adequate molecular weight and chemical structure of HBPEA. From Fig. 2(a), the observed nanostructures in P4TIF-HBPEA_ac are partly covered by the additives, so the film has low roughness and dense surface. Once the film was washed using acetone, the nanofibers are no longer obscured by the additives and become clearly visible, as shown in Fig. 2(b). This confirms that the conducting polymer is the main and fundamental component for the construction of the continuous nanofibril network. A large height difference, as in Fig. 2(b), suggests that the nanostructure provides porosity and large surface area to the conducting polymer film.

The other approach to remove the additives is to elevate the temperature near the decomposition temperature of the additives. The thermal stability of HBPEA and P4TIF was analyzed by using a thermogravimetric analyzer (TGA) and the detailed results are shown in Fig. S4(a).† The decomposition of HBPEA occurs at 242.7 °C, determined at a 5% weight loss, while P4TIF is stable during the temperature ramp until it decomposed at 405.3 °C. The P4TIF-HBPEA_TA film was annealed at 240 °C under vacuum for an hour. Fig. 2(c) shows that P4TIF-HBPEA_TA is also composed of a prominent continuous nanofibril network similar to that in P4TIF-HBPEA_w. The nanofibers are well-connected in molecular level to retain the 3D network after removing the additives. The intricate nanoscale conducting polymer network assembled by this method is not only stable in an orthogonal solvent of the conducting polymer but also endurable at high temperature of 240 °C for an hour.

To verify the removal of additives by acetone washing or thermal annealing, the exact polymer composition in the treated thin films was analyzed by using a TGA, utilizing the decomposition temperature difference in a bi-component system. The blend solution of P4TIF and HBPEA with a CP/additive ratio of 50 wt% serves as a control in this measurement. Fig. 2(d) shows the recorded weight losses of the control sample, P4TIF-HBPEA_ac, P4TIF-HBPEA_w and P4TIF-HBPEA_TA. The composition of P4TIF in P4TIF-HBPEA_ac is actually 70.3%, which is higher than the composition of P4TIF in the control, 53.0%. This can be due to the partial removal of additives by shear force during the spin-casting process. P4TIF-HBPEA_w contains 94.1% of P4TIF, indicating that more than 80.0% of HBPEA in the as-cast films have been

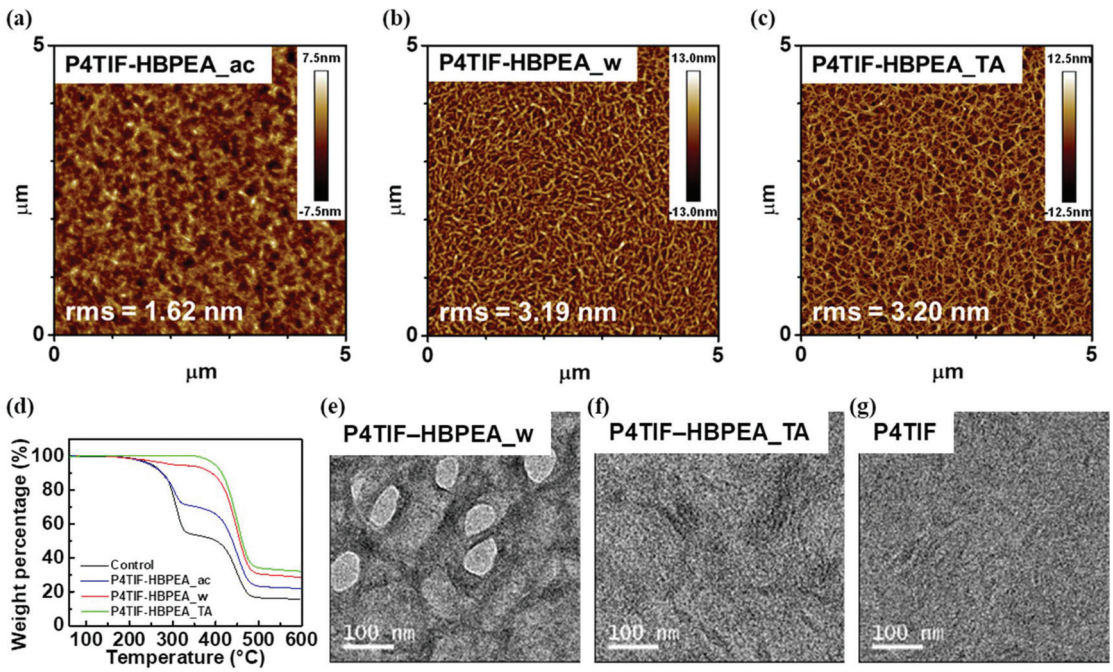

Fig. 2 Characterization of nanostructures and conducting polymer composition in the nanostructured films after removing the additives. (a–c) AFM height images of (a) P4TIF-HBPEA_ac; (b) P4TIF-HBPEA_w; and (c) P4TIF-HBPEA_TA. (d) Weight loss is determined by using a TGA of the control sample, P4TIF-HBPEA_ac, P4TIF-HBPEA_w and P4TIF-HBPEA_TA during heat treatment. (e–g) The high-resolution TEM images of (e) P4TIF-HBPEA_w, (f) P4TIF-HBPEA_TA and (g) the neat P4TIF film.

removed *via* washing with acetone. On the other hand, the calculated P4TIF composition in P4TIF-HBPEA_TA is 99.7%. Thus, thermal treatment can thoroughly remove the additives (99.0%) from the thin films and improve the crystallinity of the conducting polymers at the same time. Both the removal methods have their own merits: the use of an orthogonal solvent enables a room temperature process, while thermal annealing also promotes the molecular ordering of conducting polymers.

High-resolution transmission electron microscopy (TEM) was performed to characterize polymer nanofibers in the thin films after thermal treatment or acetone washing. There are many free spaces in the nanostructured conducting polymer films, providing contrast in the TEM image of a single-component sample. Distinct P4TIF fibers are predominantly present in the images of P4TIF-HBPEA_w and P4TIF-HBPEA_TA. As shown in Fig. 2(e), bubble-like spaces in white are present at the up-most surface and behind the dark areas of polymer fibers. This shows that free spaces are present throughout the P4TIF-HBPEA_w film and P4TIF nanofibers are interconnected to form a continuous network. Diameters of the fibers range from 13 to 69 nm with an average value of 39 nm, matching the results from the characterization of AFM. In Fig. 2(f), P4TIF nanofibers in P4TIF-HBPEA_TA are not as clear since the free spaces decrease in size during thermal treatment. Nevertheless, the average diameter of P4TIF nanofibers is 35 nm similar to that of P4TIF-HBPEA_w. The TEM image of the neat P4TIF film is shown in Fig. 2(g) for comparison. The neat P4TIF film is composed of P4TIF aggregates without any particular nanostructure, which further supports that the continuous nanofibril network results from the nanoscale phase separation of the conducting polymer and the hyperbranched polymer.

The electrical properties of CP-HBPEA films are characterized by using a thin film transistor with a bottom-gate top-contact device configuration. P4TIX polymers exhibit typical charge transport characteristics of p-type semiconductors and their electrical properties are summarized in Table S3† in the ESI. Among the three conducting polymers, P4TIF exhibits the highest hole mobility. Thus, P4TIF is chosen to study the effect of a CP/additive blending ratio and additive residual on electrical properties, and are denoted as P4F-*m*% to represent the different weight percentages of P4TIF. Five blending compositions (P4F-80%, P4F-75%, P4F-67%, P4F-50% and P4F-33%) along with neat P4TIF (P4F-100%) were investigated and the denotations of ac, w and TA are included for as-cast, acetone washing and thermal annealing, respectively. We first studied the neat conducting polymer films, P4F-100_ac and P4F-100_TA, as standard devices. Thermal annealing generally improves the charge transport of the polymer significantly. The transfer curve of P4F-100%_ac, as in Fig. 3(a), exhibits hysteresis and large resistance. After thermal annealing, hysteresis is negligible in P4F-100_TA, as shown in Fig. 3(b), and the hole mobility reaches 0.34 $cm^2\ V^{-1}\ s^{-1}$ in average, an improvement over an order in magnitude. Two reasons can be accounted for the TA effect: (1) polymer chains rearrange at a high temperature to form orderly packed crystallites and thus high crystallinity and large crystalline domains; (2) tight chains connecting crystalline and amorphous regions are closely bound to both regions. Details are discussed in the section of X-ray scattering analysis of P4TIF-HBPEA films. The FET performance of the nanostructured porous film of P4F-50%_ac, shown in Fig. 3(c),

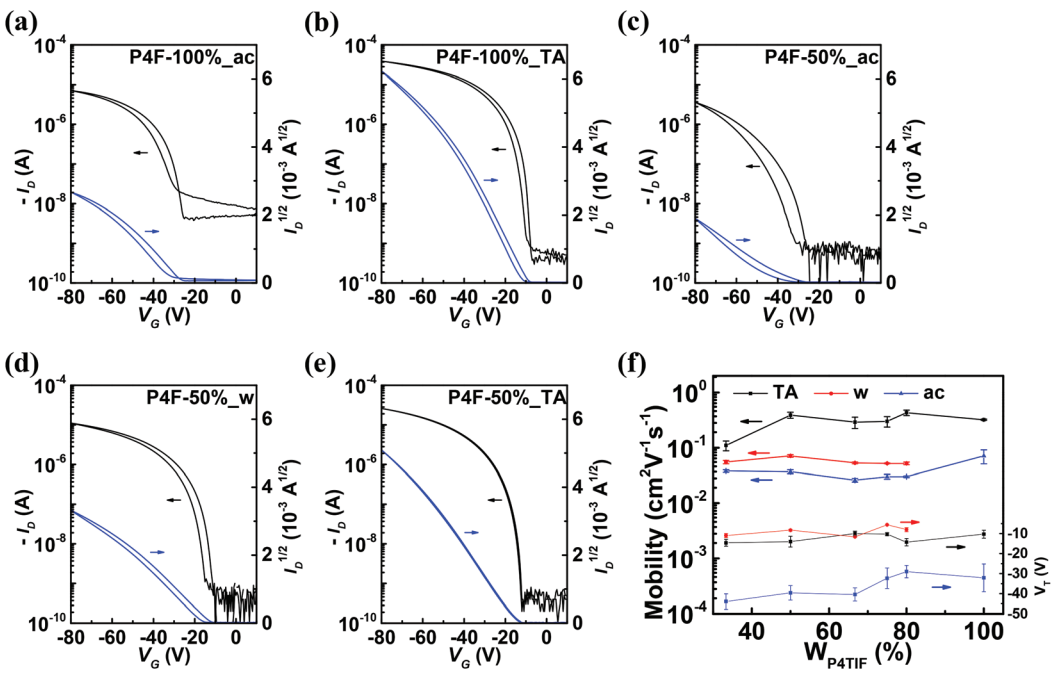

Fig. 3 Electrical performance of P4TIF-HBPEA films. (a–e) Transfer curves of (a) P4F-100%_ac, (b) P4F-100%_TA, (c) P4F-50%_ac, (d) P4F-50%_w and (e) P4F-50%_TA. (f) Mobilities and threshold voltages of P4TIF-HBPEA films.

Table 1 Summary of the P4TIF composition, FET characteristics and crystallographic parameters of P4F-HBPEA films

Sample	P4TIF content[a] [wt%]	μ_{sat} [$cm^2\ V^{-1}\ s^{-1}$]	On/off	V_T [V]	d_{100} [Å]	L_C [d] [Å]
P4F-100%_TA	100	0.34 ± 0.033	$>10^4$	−10.3 ± 2.0	27.0[b]	163
P4F-100%_ac	100	0.071 ± 0.020	$>10^3$	−32.1 ± 6.9	25.2[c]	100
P4F-50%_TA	100	0.39 ± 0.050	$>10^4$	−14.0 ± 2.7	27.2[b]	231
P4F-50%_w	94.1	0.071 ± 0.004	$>10^3$	−8.3 ± 0.4	25.8[c]	128
P4F-50%_ac	70.3	0.037 ± 0.003	$>10^3$	−39.6 ± 3.6	25.9[c]	118

[a] The composition of P4TIF is determined by using a TGA. [b] Lamellae *d*-spacing calculated by the (200) diffraction peak. [c] Lamellae *d*-spacing calculated by the (100) diffraction peak. [d] Coherence length.

is comparable to that of the compact P4F-100%_ac film. The insulating HBPEA in P4F-50%_ac does not interfere much with the charge transport of P4TIF because of the well-connected P4TIF fibers in the blend film. From the electrical properties summarized in Table 1, the turn-on voltage (V_T) and the on–off ratio of the as-cast films, however, have much room for improvement. These issues can be solved by removing HBPEA from P4F-HBPEA blends. P4F-50%_w exhibits well-defined V_T with values close to those of devices with TA treatment. V_T depends strongly on the joint connection between crystalline and amorphous regions of the polymer. Once HBPEA is removed from the connection point, the insulating HBPEA no longer imposes additional resistance in the film, and thus the macroscopic charge transport in P4F-50%_w is similar to P4F-50%_TA.

To evaluate the impact of the conducting polymer composition on charge transport, electrical properties of blend films with various blending ratios are shown in Fig. 3(f). In the comparison between as-cast P4TIF-HBPEA films and P4F-100%_ac, the presence of HBPEA slightly decreases the macroscopic mobility of blend films and the V_T value increases with decreasing P4TIF composition. As an insulator well-blended with P4TIF, HBPEA increases the resistance of as-cast films and builds up the energy barrier of charge transport in the conducting polymer. These side effects associated with HBPEA are rectified once HBPEA is removed. The acetone-washed P4TIF-HBPEA films have mobilities independent of the composition of P4TIF (from 33% to 80%), and their transfer characteristics are similar to those of TA devices, including negligible hysteresis and a turn-on voltage −8.3 V. On the other hand, the devices with thermal annealing treatment show similar performance to P4F-100%_TA. By removing the additives with acetone or thermal treatment, the charge transport in P4TIF is not affected by the blending composition in the investigated range and the corresponding morphology change.

To study the effect of additives on the formation of conducting polymer crystallites, GIWAXS was performed for the P4TIF-HBPEA films. From the 2D GIWAXS images in Fig. 4(a–e), the signals in the Q_z direction correspond to the edge-on lamellae structures of P4TIF. The polymer alkyl chains packed perpendicular to the substrate is called an edge-on packing orientation, which is beneficial for the charge carrier transport in FET. As shown in Fig. 4(a–c), polymers are packed only in the edge-on orientation in P4F-50%_ac, P4F-50%_w and P4F-50%_TA films. Thus, blending with HBPEA and forming a fibril network do not affect the packing orientation of P4TIF. For P4F-50%_TA and P4F-100%_TA, the thermal treatment increases the crystallinity and packing order of polymer crystallites, and the (300) high-order reflection spots can be observed in Fig. 4(c) and (e).

Fig. 4(f) shows the 1D scattering profiles integrated from the line-cuts of 2D GIWAXS images in the Q_z-direction. Highly crystalline polymer crystallites are present in both TA films, accounting for the strong scattering intensity and high-order reflection. In contrast, the weak and broad lamellae (100) peaks of the films without TA suggest that P4TIF merely packs loosely to form aggregates during film formation. The lamellae spacing (d_{100}) of P4TIF can be determined by the (100) peak position. Interestingly, P4F-100%_TA and P4F-50%_TA have larger d_{100} than those without TA because of the rearrangement of alkyl side chains during thermal annealing. The alkyl chains are interdigitated in thin films processed only at room temperature. Chain rearrangement induced by thermal annealing increases the ordering of polymer packing and disentangles the interdigitated chains in the process. On another note, P4F-50%_ac has a d_{100} of 25.8 Å, slightly larger than the d_{100} of P4F-100%_ac, indicating that blending with HBPEA slightly disentangles the interdigitated chains. Detailed calculated crystallographic parameters are summarized in Table 1. The crystallinity of conducting polymers without and with additives can show differences in the crystallite (orderly packed lamellae) size of P4TIF in the P4TIF film and P4TIF-HBPEA films. Since polymers are polycrystalline, correlation length (L_C) is used to quantitatively analyze the size of a crystallite.[47] The L_C is calculated using the following formula:

$$L_C = \frac{2\pi}{Q_{FWHM}} \quad (1)$$

The calculated L_C values are 100, 118 and 128 Å for P4F-100%_ac, P4F-50%_ac and P4F-50%_w films, respectively. Large L_C and thus large crystalline domain size in P4TIF-HBPEA further support that HBPEA reinforces the crystallinity in P4TIF crystallites and aggregates. For a room temperature process, this is a powerful method to improve the quality of polymer aggregates. Similarly in thermally annealed films, P4F-100%_TA and P4F-50%_TA films have the L_C values of 163 and 231 Å, respectively. Such results strongly support the idea that the

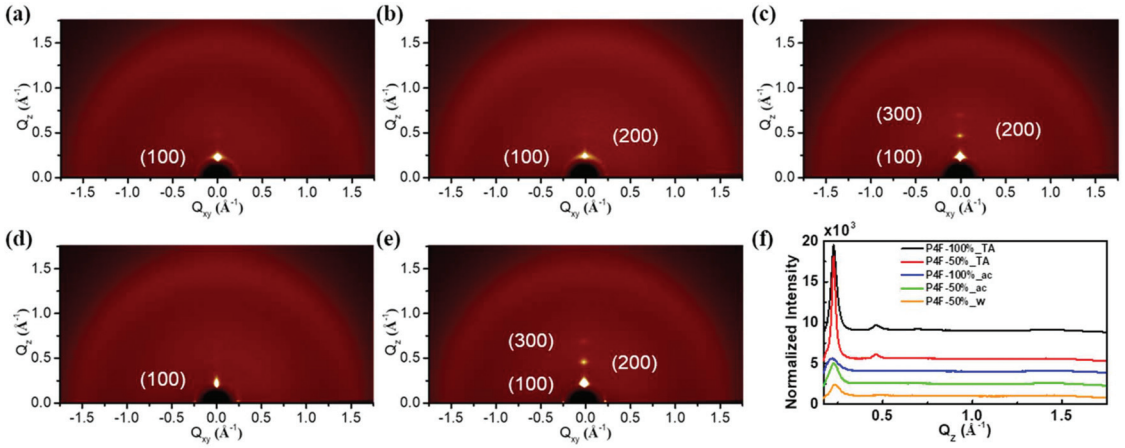

Fig. 4 X-ray scattering analysis of P4TIF-HBPEA films. (a–e) 2D grazing-incidence wide-angle X-ray scattering (GIWAXS) images of (a) P4F-50%_ac, (b) P4F-50%_w, (c) P4F-50%_TA, (d) P4F-100%_ac and (e) P4F-100%_TA. (f) 1D GIWAXS profiles integrated along the out-of-plane direction.

HBPEA additive improves the crystallinity of the conducting polymer.

To demonstrate the advantages of a continuous fibril network, we fabricated a high-sensitivity ammonia sensor by using P4F-50%_TA FET. Ammonia gas generally acts as a trap for p-type semiconductors, decreasing the gate-induced drain current. Therefore, the sensing response is defined according to the measured drain current changes, as:

$$R = \frac{I_D(0) - I_D(t)}{I_D(0)} \quad (2)$$

where $I_D(t)$ and $I_D(0)$ are the drain current at time t and the beginning of the measurement, respectively. Dry air was used as a carrier gas for the measurement. The sensors were exposed to ammonia gas of concentrations ranging from 20 ppb to 5 ppm in a 30 s interval alternating with 30 s flushing of dry air. The response time (t_{90}) is used to define the time when the signals reach 90% of the saturated value. Real-time sensing results of P4F-50%_TA and P4F-100%_TA are shown in Fig. 5(a). P4F-100%_TA can detect 200 ppb of ammonia in 29.0 s but the signals are obscured by the fluctuation upon exposure to ammonia concentrations of 100 ppb and below. In comparison, P4F-50%_TA exhibits a faster and larger response to the uptake of ammonia that is two magnitudes higher than that of P4F-100%_TA due to the large surface area of the nanofibril network. P4F-50%_TA can detect 100 ppb of ammonia in 25.8 s, a commendable sensing performance for polymer-based sensors. To explore the possibility of the room temperature process, we employed polymer transistors without thermal treatment in real-time ammonia sensing. P4F-100%_ac and P4F-50%_w were tested by using a similar procedure and the sensing results are shown in Fig. 5(b). When the sensors are exposed to an ammonia environment, they show similar response time, response magnitude and the lowest detected concentration of 200 ppb. Besides surface area, the crystallinity and hole mobility of polymer crystallites and aggregates also play important roles in FET-based sensors. P4F-100%_ac and P4F-50%_w practically match in terms of crystallinity and FET mobility, and the large surface area of P4F-50%_w does not lead to an apparent improvement in sensing ammonia. This is because there are amorphous P4TIF covering the aggregated P4TIF and ammonia molecules cannot

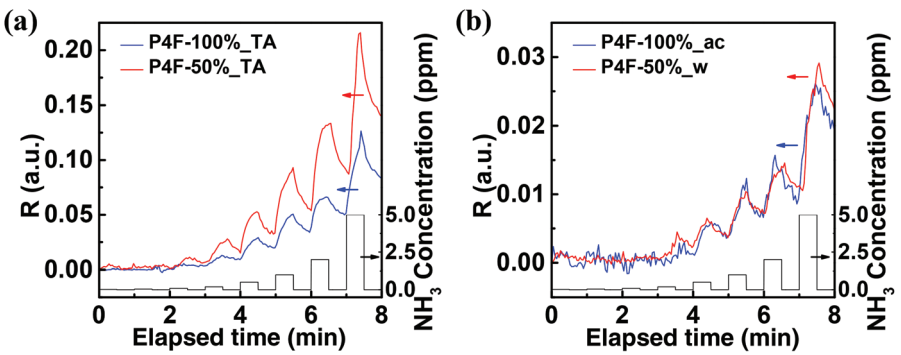

Fig. 5 Highly sensitive ammonia sensors fabricated from the nanostructured P4TIF film. Real-time ammonia sensing response of (a) P4F-100_TA and P4F-50_TA and (b) P4F-100_ac and P4F-50_w FETs exposed to various concentrations of ammonia ranging from 20 ppb to 5 ppm. Dry air served as a carrier gas.

efficiently trap the charge carriers in the conducting channels. The polymer crystallinity and packing order also account for the greater sensitivity of TA devices compared to the room temperature processed sensors.

Conclusion

In this study, we investigated the use of hyperbranched polymers as additives for preparing stable nanostructures in conducting polymer films. Nanoscale phase separation of two blending components introduces a continuous nanofibril network into thin films with tightly connected polymer chains to obtain excellent charge transport. The nanofibril network in conducting polymers constructed *via* the proposed approach remains intact after thermal treatment and exposure to an orthogonal solvent of the conducting polymer. We explored this method in ammonia detection to achieve a fast-responded and highly sensitive sensor *via* the large surface area provided by the nanostructures. An assembled P4TIF FET with a continuous nanofibril network can detect 100 ppb of ammonia in air in less than 26 s. We provided insights into the relationship between the surface area of thin films, mobility of the semiconducting polymers and sensibility of ammonia sensors. This general approach can pave the way for the development of nanostructured polymer thin films for applications in electronics, catalysts, batteries and sensors.

Experimental

Materials

P4TIH, P4TIF and P4TIN were synthesized by Stille coupling, according to our previous report.[41–43] In short, bithiophene, difluorobithiophene and dicyanobithiophene were first modified with trimethyltin and the isoindigo moiety was flanked by two 3-dodecyl thiophene spacers before polymerization. The number-average molecular weight (M_n) and the molecular weight distribution (PDI) of P4TIH, P4TIF and P4TIN are in the range of 60–109 kDa and 1.6–2.5, respectively. Gel permeation chromatography (GPC) was performed to evaluate these values at 40 °C, using chloroform as an eluent and monodisperse polystyrene as a calibration standard. Hyperbranched polyesteramide Hybrane® HV 2680 was purchased from Polymer Factory. Other chemical reagents were purchased from suppliers and used as received, unless mentioned otherwise.

Device fabrication

Polymer thin film transistors featuring a bottom-gate and top-contact geometry were fabricated on highly doped n-type silicon with 300 nm of thermal oxide. The substrate was modified with a self-assembled monolayer by using the following procedure. The silicon wafer was first cleaned by oxygen plasma for 15 min and a solution of 3.0 mM trimethoxy (octadecyl)silane in anhydrous trichloroethylene was spin-cast on the wafer. The OTS-covered wafer was treated with ammonia vapor for 12 h, followed by cleaning with toluene, ethanol and acetone by using an ultrasonicator. Conducting polymers were dissolved in chloroform with a concentration of 0.10 wt%, and the blending solutions were prepared by adding additional HBPEA with a concentration of 0.025, 0.050, 0.067, 0.100 and 0.200 wt% in the solution for P4F-80%, P4F-75%, P4F-67%, P4F-50% and P4F-33%, respectively. The polymer films or hybrid films were fabricated by the spin-coating process from the respective solutions onto the OTS-modified substrates at 800 rpm for 1 min in a nitrogen environment. The as-cast films were dipped in acetone for 15 min to remove HBPEA from the thin films, followed by blowing with N_2 flow gently. The thermal treatment of the thin films was performed at 240 °C under vacuum for an hour and the polymer films were slowly cooled to room temperature. Au source/drain electrodes of 100 nm were thermally evaporated on thin films through shadow masks, and the prepared FET devices feature the channel length (L) of 100 μm and the channel width (W) of 1 mm.

Measurement

Thermal properties of P4TIF and HBPEA were analyzed by using a thermogravimetric analyzer (Pyris 1 TGA, PerkinElmer, US). The thermal stabilities of the samples under nitrogen were determined by their weight losses at 5 wt% during ramping from 60 °C to 600 °C at a rate of 10 °C min^{-1}. The composition of HBPEA in the blend solution, as-cast films, thermally annealed films and acetone-washed films was determined by using a TGA. P4F-50% was used as an example in this analysis. Samples for TGA were prepared by using different methods: the blend solution was drop-cast on silicon wafer and peeled off after drying under vacuum for 12 h for the sample of the blend solution; the drop-cast films were annealed at 240 °C for an hour and peeled off for the thermally annealed sample; the sample of as-cast films was collected from 30 spin-cast films by dissolving in chloroform and drying under vacuum; the acetone-washed sample was collected from 50 spin-cast films after acetone treatment in a similar procedure. High-resolution images of thin films were obtained by using a transmission electron microscope (JEM-1400, JEOL, Japan), operating at 120 kV in a bright-field mode. TEM samples were prepared in a similar manner to FET devices but using a different substrate. A water-soluble poly(3,4-ethylenedioxythiophene) polystyrene sulfonate (PEDOT:PSS, AI4083) layer was spin-cast on silicon wafer at 1000 rpm for 30 s, followed by annealing at 150 °C for 10 min before the deposition of the polymer or hybrid films. As-cast films, annealed films and acetone-washed films were dipped in deionized water to separate the polymer/hybrid films from silicon substrates. The thin films were transferred to cupper grids and stored under vacuum for 12 h before the TEM experiment. The surface morphology of polymer thin films was probed by tapping mode of atomic force microscopy (OMV-NTSC, Bruker, US). Grazing-incidence wide-angle X-ray scattering (GIWAXS) analysis was performed at beamline 13A and 17A in the National Synchrotron Radiation Research Center (NSRRC) in Taiwan.

The thin films were carefully aligned and adjusted to afford an X-ray incident angle of 0.2° for each measurement. The signals were collected by a Mar165 or a Mar345 CCD detector. The thin films for AFM and GIWAXS measurements were prepared by using the same method as for FET devices prior to the deposition of top electrodes.

The electrical properties of P4F-HBPEA FETs were measured by a precision source/measurement unit (B2912A, Keysight, US) with the support of a probe station or a temperature controlled stage (Linkam Scientific, UK). The mobility (μ) at the saturation region was calculated by using the following formula:

$$\mu_{sat} = \frac{\left(\frac{d\sqrt{I_{SD}}}{dV_{SG}}\right)^2}{\frac{1}{2}C_i\frac{W}{L}} \quad (3)$$

where I_{SD} is the source–drain current; V_{SG} is the source–gate voltage; C_i is the dielectric constant of SiO_2; and W and L are the channel width and length. For ammonia detection, the FETs were measured in an air-tight sealing temperature-controlled stage. Various concentrations of ammonia environments were prepared by diluting ammonia/air standard of 15 ppm with a carrier gas (dry air) using mass flow controllers (Alicat, US). The prepared ammonia mixture was concurrently transferred into the temperature-controlled stage, where the sensor operates at 25 °C and 1 atm.

Conflicts of interest

There are no conflicts to declare.

Acknowledgements

The authors thank the Ministry of Science and Technology in Taiwan for financial support under the grants of MOST 107-2221-E-002-005, MOST 108-3017-F-002-002 and MOST 107-2119-M-002-012. Thanks are also due to the "Advanced Research Center of Green Materials Science and Technology" from The Featured Area Research Center Program within the framework of the Higher Education Sprout Project by the Ministry of Education (107L9006). The authors thank Mr Shih-Hsin Huang (Institute of Chemistry, Academia Sinica) for the support of TEM operation.

References

1 Y. H. Lee, O. Y. Kweon, H. Kim, J. H. Yoo, S. G. Han and J. H. Oh, *J. Mater. Chem. C*, 2018, **6**, 8569–8612.
2 S. Zhang, Y. Zhao, X. Du, Y. Chu, S. Zhang and J. Huang, *Small*, 2019, **15**, e1805196.
3 Z. Ma, P. Chen, W. Cheng, K. Yan, L. Pan, Y. Shi and G. Yu, *Nano Lett.*, 2018, **18**, 4570–4575.
4 A. M. Bryan, L. M. Santino, Y. Lu, S. Acharya and J. M. D'Arcy, *Chem. Mater.*, 2016, **28**, 5989–5998.
5 J. Wu, X. Rui, C. Wang, W.-B. Pei, R. Lau, Q. Yan and Q. Zhang, *Adv. Energy Mater.*, 2015, **5**, 1402189.
6 J. Wang, J. Wang, Z. Kong, K. Lv, C. Teng and Y. Zhu, *Adv. Mater.*, 2017, **29**, 1703044.
7 D. Xu, L. Fan, L. Gao, Y. Xiong, Y. Wang, Q. Ye, A. Yu, H. Dai, Y. Yin, J. Cai and L. Zhang, *ACS Appl. Mater. Interfaces*, 2016, **8**, 17090–17097.
8 C. Kleber, M. Bruns, K. Lienkamp, J. Ruhe and M. Asplund, *Acta Biomater.*, 2017, **58**, 365–375.
9 S. Ghosh, N. A. Kouame, L. Ramos, S. Remita, A. Dazzi, A. Deniset-Besseau, P. Beaunier, F. Goubard, P. H. Aubert and H. Remita, *Adv. Mater.*, 2015, **14**, 505–511.
10 S. Ghosh, T. Maiyalagan and R. N. Basu, *Nanoscale*, 2016, **8**, 6921–6947.
11 D. N. Nguyen and H. Yoon, *Polymers*, 2016, **8**, 118.
12 L. J. Pan, L. Pu, Y. Shi, S. Y. Song, Z. Xu, R. Zhang and Y. D. Zheng, *Adv. Mater.*, 2007, **19**, 461–464.
13 M. J. Antony and M. Jayakannan, *J. Phys. Chem. B*, 2007, **111**, 12772–12780.
14 R. Liu, J. Duay and S. B. Lee, *ACS Nano*, 2011, **5**, 5608–5619.
15 R. Hassanien, M. Al-Hinai, S. A. Farha Al-Said, R. Little, L. Šiller, N. G. Wright, A. Houlton and B. R. Horrocks, *ACS Nano*, 2010, **4**, 2149–2159.
16 F. Zhang, G. Qu, E. Mohammadi, J. Mei and Y. Diao, *Adv. Funct. Mater.*, 2017, **27**, 1701117.
17 O. Y. Kweon, M. Y. Lee, T. Park, H. Jang, A. Jeong, M.-K. Um and J. H. Oh, *J. Mater. Chem. C*, 2019, **7**, 1525–1531.
18 L. Pan, G. Yu, D. Zhai, H. R. Lee, W. Zhao, N. Liu, H. Wang, B. C. Tee, Y. Shi, Y. Cui and Z. Bao, *Proc. Natl. Acad. Sci. U. S. A.*, 2012, **109**, 9287–9292.
19 Y. Wang, Y. Shi, L. Pan, Y. Ding, Y. Zhao, Y. Li, Y. Shi and G. Yu, *Nano Lett.*, 2015, **15**, 7736–7741.
20 X. Wang, W. H. Lee, G. Zhang, X. Wang, B. Kang, H. Lu, L. Qiu and K. Cho, *J. Mater. Chem. C*, 2013, **1**, 3989–3998.
21 D. Choi, H. Kim, N. Persson, P.-H. Chu, M. Chang, J.-H. Kang, S. Graham and E. Reichmanis, *Chem. Mater.*, 2016, **28**, 1196–1204.
22 S. Wu, G. Wang, Z. Xue, F. Ge, G. Zhang, H. Lu and L. Qiu, *ACS Appl. Mater. Interfaces*, 2017, **9**, 14974–14982.
23 F. Ge, Z. Liu, S. B. Lee, X. Wang, G. Zhang, H. Lu, K. Cho and L. Qiu, *ACS Appl. Mater. Interfaces*, 2018, **10**, 21510–21517.
24 M. Selivanova, C. H. Chuang, B. Billet, A. Malik, P. Xiang, E. Landry, Y. C. Chiu and S. Rondeau-Gagne, *ACS Appl. Mater. Interfaces*, 2019, **11**, 12723–12732.
25 Z. He, J. Chen and D. Li, *Soft Matter*, 2019, **15**, 5790–5803.
26 H.-C. Liao, C.-C. Ho, C.-Y. Chang, M.-H. Jao, S. B. Darling and W.-F. Su, *Mater. Today*, 2013, **16**, 326–336.
27 J. Chen, Z. Bi, X. Xu, Q. Zhang, S. Yang, S. Guo, H. Yan, W. You and W. Ma, *Adv. Sci.*, 2019, **6**, 1801560.
28 J. Yuan, Y. Xu, G. Shi, X. Ling, L. Ying, F. Huang, T. H. Lee, H. Y. Woo, J. Y. Kim, Y. Cao and W. Ma, *J. Mater. Chem. A*, 2018, **6**, 10421–10432.
29 M. S. Park and F. S. Kim, *Polymers*, 2019, **11**, 112.

30 S.-F. Liao, C.-F. Lu, A. D. Fenta, C.-T. Chen, C.-Y. Chao and W.-F. Su, *J. Mater. Chem. A*, 2019, **7**, 21309–21320.
31 C.-C. Ho, Y.-H. Lee, C.-A. Dai, R. A. Segalman and W.-F. Su, *Macromolecules*, 2009, **42**, 4208–4219.
32 C. A. Dai, W. C. Yen, Y. H. Lee, C. C. Ho and W. F. Su, *J. Am. Chem. Soc.*, 2007, **129**, 11036–11038.
33 Y. Mai and A. Eisenberg, *Chem. Soc. Rev.*, 2012, **41**, 5969–5985.
34 Y. Zheng, S. Li, Z. Weng and C. Gao, *Chem. Soc. Rev.*, 2015, **44**, 4091–4130.
35 S. B. Kharchenko, R. M. Kannan, J. J. Cernohous and S. Venkataramani, *Macromolecules*, 2003, **36**, 399–406.
36 Y. H. Kim, *J. Polym. Sci., Part A: Polym. Chem.*, 1998, **36**, 1685–1698.
37 M. Johansson, in *Encyclopedia of Materials: Science and Technology*, ed. K. H. J. Buschow, R. W. Cahn, M. C. Flemings, B. Ilschner, E. J. Kramer, S. Mahajan and P. Veyssière, Elsevier, Oxford, 2001, pp. 7673–7675, DOI: 10.1016/B0-08-043152-6/01372-3.
38 C.-F. Lu, C.-W. Shih, C.-A. Chen, A. Chin and W.-F. Su, *Adv. Funct. Mater.*, 2018, **28**, 1803145.
39 C. Grand, S. Baek, T.-H. Lai, N. Deb, W. Zajaczkowski, R. Stalder, K. Müllen, W. Pisula, D. G. Bucknall, F. So and J. R. Reynolds, *Macromolecules*, 2016, **49**, 4008–4022.
40 T. Lei, J. Y. Wang and J. Pei, *Acc. Chem. Res.*, 2014, **47**, 1117–1126.
41 S.-F. Liao, C.-T. Chen and C.-Y. Chao, *ACS Macro Lett.*, 2017, **6**, 969–974.
42 C.-C. Ho, C.-A. Chen, C.-Y. Chang, S. B. Darling and W.-F. Su, *J. Mater. Chem. A*, 2014, **2**, 8026–8032.
43 C.-F. Lu, S.-F. Liao, I.-F. Chen, C.-T. Chen, C.-Y. Chao and W.-F. Su, *ACS Appl. Electron. Mater.*, 2019, **1**, 1873–1880.
44 Y. Lei, P. Deng, J. Li, M. Lin, F. Zhu, T. W. Ng, C. S. Lee and B. S. Ong, *Sci. Rep.*, 2016, **6**, 24476.
45 X. Guo, H. Xin, F. S. Kim, A. D. T. Liyanage, S. A. Jenekhe and M. D. Watson, *Macromolecules*, 2011, **44**, 269–277.
46 X. Qiao, Q. Wu, H. Wu, J. Zhang and H. Li, *Adv. Funct. Mater.*, 2017, **27**, 1604286.
47 J. Rivnay, S. C. Mannsfeld, C. E. Miller, A. Salleo and M. F. Toney, *Chem. Rev.*, 2012, **112**, 5488–5519.